Int. J. Heat Mass Transfer. Vol. 28, No. 10, pp. 1907–1920, 1985
Printed in Great Britain

0017–9310/85 $3.00 + 0.00
Pergamon Press Ltd.

Subcooled flow boiling at high heat flux

VICTOR H. DEL VALLE M.* and D. B. R. KENNING
Department of Engineering Science, Oxford University, Parks Road, Oxford, U.K.

(*Received* 22 *October* 1984 *and in final form* 15 *May* 1985)

Abstract—In an experimental investigation of subcooled flow nucleate boiling of water at atmospheric pressure on stainless steel it was found that the heat transfer coefficient increased with increasing subcooling and also with increasing wall thickness over the range 0.08–0.20 mm. Bubble size, frequency and the distribution of nucleation sites were measured at 1.7 m s^{-1} inlet velocity, 84 K subcooling, 0.08-mm wall thickness and heat fluxes 70–95% of the critical flux. The observations were consistent with a model for heat transfer primarily by surface quenching at the bubble frequency, supplemented by single-phase convection and a small contribution from microlayer evaporation. Although the total population of nucleation sites increased with increasing wall superheat, the startup of new sites deactivated many of the sites active at lower superheat.

1. INTRODUCTION

THE CLEAR view of the surface which can be obtained in subcooled flow boiling, even at high heat flux, offers some experimental advantages over pool boiling for the examination of unresolved questions concerning the mechanism of heat transfer in nucleate boiling. The reputed insensitivity of the heat transfer coefficients in nucleate boiling to flow and subcooling gives reason to hope that conclusions drawn from subcooled boiling may be of more general application.

The observations reported in this paper were taken incidentally to a study of the effect of wall thickness on the critical heat flux in subcooled flow boiling of water at atmospheric pressure [1]. Boiling curves were measured at fixed flow rate and inlet subcooling with gradual increases in heat flux until destruction of the test surface occurred. Consequently hysteresis and boiling with decreasing flux were not examined. The test surfaces were stainless-steel plates, heated by direct electrical current over an area 150 × 10 mm, set into one side of a vertical flow channel of rectangular cross-section 12 × 5 mm. Three wall thicknesses (nominal values 0.08, 0.13 and 0.20 mm), three values of inlet velocity (0.8, 1.7 and 2.0 m s^{-1}) and three values of inlet subcooling (24, 54 and 84 K) were employed. Boiling curves were measured for all combinations of these variables and cine films were taken at 10,000 f.p.s. through a window opposite the test surface to determine the flow regimes. For one set of conditions (0.08-mm wall thickness, 1.7 m s^{-1}, 84 K subcooling) the films taken at heat fluxes of 70, 80, 90 and 95% of the critical flux (4.92 MW m^{-2}) were analysed in detail to obtain the bubble size, frequency and lifetime and the positions of all active nucleation sites in an area 10 mm square. The large time required for film analysis has so far prevented the examination of other conditions in similar detail.

In boiling experiments it is convenient to use thin-walled test sections heated by the direct passage of electrical current. However, it is known that the thickness of the wall affects the critical heat flux in pool [2] and flow [3–5] boiling. Examinations of the effect of wall thickness on the nucleate boiling curve have been confined to pool boiling [6–8]. The disagreement about whether heat transfer coefficients are bigger or smaller on thin walls [8] may in part be due to experimental difficulties. The problems of measuring and interpreting the temperatures of thin walls are discussed in [9]. Another problem is the effect of variations in surface conditions: for our flow boiling experiments the surface conditions of wall materials of different thickness were shown to be similar by conventional measurements of roughness and by experiments on the isothermal nucleation of gas bubbles from supersaturated solutions. By comparing various combinations of conditions we have been able to identify the separate effects of flow rate, subcooling and wall thickness on nucleate boiling heat transfer.

The development of design formulae for nucleate boiling heat transfer may involve semi-empirical correlations (which cannot readily incorporate the effects of surface conditions), or mechanistic models which at present have to use experimental data or empirical correlations for nucleation site densities and bubble growth parameters. Our detailed analysis of four cine films is intended to contribute to the mechanistic approach. A previous study [10] suggested that the nucleation site density did not depend simply on the size distribution of cavities present on the surface. We have looked particularly for evidence of interference between adjacent sites which would modify the active site density. The measurements of site densities and bubble behaviour have been fed into a simple heat transfer model of a type used by other workers e.g. [11]: an area of influence round each

* Present address: Instituto Nacional de Investigaciones Nucleares, Agricultura 21, Col. Escandón, México 18, D.F., 11800 Mexico.

NOMENCLATURE

b	$Ja\,\alpha_l^{1/2}$
c	specific heat
F	$\pi R_m^2 n$
Ja	Jacob number, $\rho_l c_l \Delta T_{SAT}/\rho_v \lambda$
k	thermal conductivity
K	ratio area of influence to projected area
n	nucleation site density
P	probability density
Pr	Prandtl number, ν_l/α_l
R	radius
R_m	maximum bubble radius
s	nearest-neighbour distance
t	time
t_0	time during bubble growth
t^+	$t_0\sigma^2/b^6\rho_l^2$
t_D	delay time, microlayer evaporation
t_E	evaporation time, microlayer evaporation
t_L	bubble lifetime
t_P	bubble period
t_Q	quench time
ΔT	temperature difference
ΔT_{SAT}	wall superheat
ΔT_{SUB}	liquid subcooling
X	ratio true to nominal boiling area.

Greek symbols

α	thermal diffusivity
δ	wall thickness
δ_M	microlayer thickness
δ_{MO}	initial microlayer thickness
ε	decrease in microlayer thickness during t_D
λ	latent heat of evaporation
ν	kinematic viscosity
ρ	density
σ	surface tension
ϕ	heat flux
ϕ_C	convective heat flux
ϕ_{NB}	nucleate boiling heat flux
ϕ_{NBI}	nucleate boiling heat flux at inception
$\bar{\phi}_Q$	mean quenching heat flux.

Subscripts

l	liquid
v	vapour.

nucleation site is repeatedly quenched at the bubble frequency by liquid at the bulk temperature; heat transfer under the bubbles is modified by microlayer evaporation and the wall between areas of influence is cooled by single-phase convection. We have removed some anomalies in the divisions between the three modes of heat transfer and we have incorporated an allowance for overlapping areas of influence, discussed in [12].

As noted above, detailed analysis has been performed only for one combination of flow rate and subcooling on the thinnest wall. It has been suggested that bubble growth is modified on very thin walls in pool boiling [6] so our data may not be applicable to other conditions.

2. EXPERIMENTAL PROCEDURES

2.1. *Flow boiling rig and test section*

The boiling heat transfer rig delivered double-distilled, degassed water to the test section at controlled conditions of flow rate, temperature and pressure. The rig was pressurised by a vessel containing boiling water vented to the atmosphere, situated 1.6 m above the test section. The saturation temperature at the test section was 104.0°C. (The wall superheats in [1] based on a saturation temperature of 100°C have been corrected here for the additional hydrostatic head.) The rig and the general construction of the test section have been described elsewhere [1, 13]. The test surface was heated by direct current from a three-phase full-wave rectifier.

2.2. *Test surfaces*

The test surfaces were cut from sheets of hard-rolled semi-polished stainless steel (BS1449 EN58A) from the same manufacturer. They were not subjected to any treatment other than cleaning with acetone followed by detergent in hot water and a final rinse in double-distilled water. Samples from each sheet had the following values of CLA surface roughness measured by Talysurf: 0.08 mm, 0.152 μm; 0.13 mm, 0.152 μm; 0.20 mm, 0.112 μm. Surface roughness may be a poor guide to bubble nucleation characteristics so the densities of stable nucleation sites on samples of each material were determined by observations of gas bubble nucleation following sudden depressurisation with the surfaces immersed in water saturated with nitrogen at 25°C. The technique is described fully in [13, 14]. The measurements suggest that the three surfaces have similar nucleation characteristics and respond in a similar way to prepressurisation, which simulates subcooling prior to superheating, Fig. 1.

2.3. *Wall temperature measurement*

Wall temperatures were measured by five copper–constantan thermocouples individually calibrated to ± 0.1 K. The thermocouples were glued to the adiabatic rear surface of the heated wall with a thin film of epoxy cement, then covered with a 3-mm-thick layer of silicone rubber backed by a 6-mm-thick strip of asbestos-based insulating board. Electrical guard heaters were adjusted to maintain the rear surface of this strip at the same temperature as the wall thermocouples so that

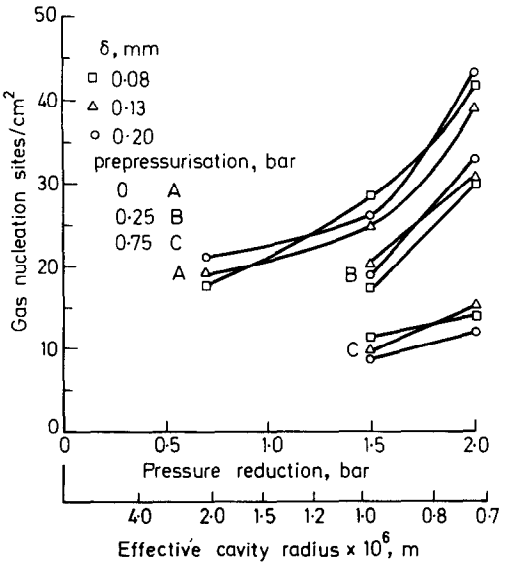

FIG. 1. Gas bubble nucleation characteristics of the three surfaces.

there was no temperature gradient across the epoxy layer which insulated the thermocouples electrically from the wall.

The measurements were corrected in the usual way for the temperature difference across the wall, by subtracting

$$T = \frac{\phi\delta}{2k}. \quad (1)$$

The thermal conductivity of the stainless steel was measured as 16 W m^{-1} K^{-1} ±5% [14]. The wall thicknesses were measured by micrometer, the accurate values being 0.076, 0.127 and 0.203 mm, all ±0.003 mm. Between the minimum and maximum thicknesses, the greatest difference in the wall superheat attributable to these uncertainties is 1 K at a heat flux of 5×10^6 W m^{-2}, being proportional to the heat flux.

During nucleate boiling on a very thin wall, it is likely that the temperature of the rear adiabatic surface will vary with time at the bubble frequency (about 500 Hz in this study) and on a length scale equal to the distance between active nucleation sites (about 0.5 mm). The measuring system averages out the fluctuating component and, as discussed in [9], the method of attaching the thermocouples averages out the spatial variations to some extent. However, there remains a possibility that the temperature recorded by a wall thermocouple might depend on its precise position relative to an active nucleation site. The circumstantial evidence that this was not a problem in this study is:

(i) agreement to ±0.5 K between the two upper thermocouples on each test surface;
(ii) the smooth increase in wall temperature as the heat flux is increased in small steps;
(iii) agreement between boiling curves to ±0.5 K when some runs were repeated to or three times with fresh test surfaces.

Therefore it is assumed that the measurements of the wall rear adiabatic temperature represent mean values with respect to both time and position.

3. BOILING CURVES

3.1. *Experimental data*

The 27 boiling curves are presented in Fig. 2. For any given conditions of liquid flow rate and temperature, the boiling curve for the 0.08-mm wall lies 3–5 K to the right of the curve for the 0.20-mm wall. The difference does not increase in proportion to the heat flux and exceeds the difference which could be caused by the uncertainties in wall thickness and conductivity (Section 2.3). It might be caused by differences in surface finish on the three sheets of stainless steel from which the test surfaces were cut: this cannot be ruled out conclusively but it has been shown that the sheets had similar roughness and bubble nucleation characteristics (Section 2.2). Thus it is likely that variations of 10–25% in wall superheat can be attributed to the influence of wall thickness.

Superimposed on each set of boiling curves is the extrapolation of the measured single-phase forced convection curve. The measurements agreed to ±7% with the correlation of James *et al.* [15] for asymmetrically heated rectangular ducts, whereas conventional correlations for round tubes overestimated the heat transfer rate by 10–25% [16].

3.2. *The nucleate boiling curve*

Many flow boiling correlations employ superposition of a convective heat flux ϕ_C and a nucleate boiling flux ϕ_{NB}, e.g. Bjorge *et al.* [17] propose for subcooled boiling

$$\phi = [\phi_C^2 + (\phi_{NB} - \phi_{NB1})^2]^{1/2} \quad (2)$$

where ϕ_C is obtained from a correlation for single-phase convection, ϕ_{NB} is given by a 'fully-developed nucleate boiling curve', supposed to be insensitive to the cavity size distribution on the surface, and ϕ_{NB1} is the flux on that curve at a predicted superheat for the inception of nucleation (which does depend on the available cavity sizes). This correlation overpredicts the wall superheats measured in this study by a large margin (Fig. 2), throwing doubt on the assumption that the nucleate flow boiling flux is insensitive to the distribution of nucleation sites. Further experimental investigation of this question is required. Meanwhile the importance of comparing the nucleation characteristics of test surfaces of different thicknesses, when attempting to isolate any effect of thickness on nucleate boiling, is underlined.

The general principle of superposition may be satisfactory despite the difficulty of specifying the right nucleate boiling curve. Here we test the principle by deducing nucleate boiling curves $\phi_{NB}(\Delta T_{SAT})$ from the

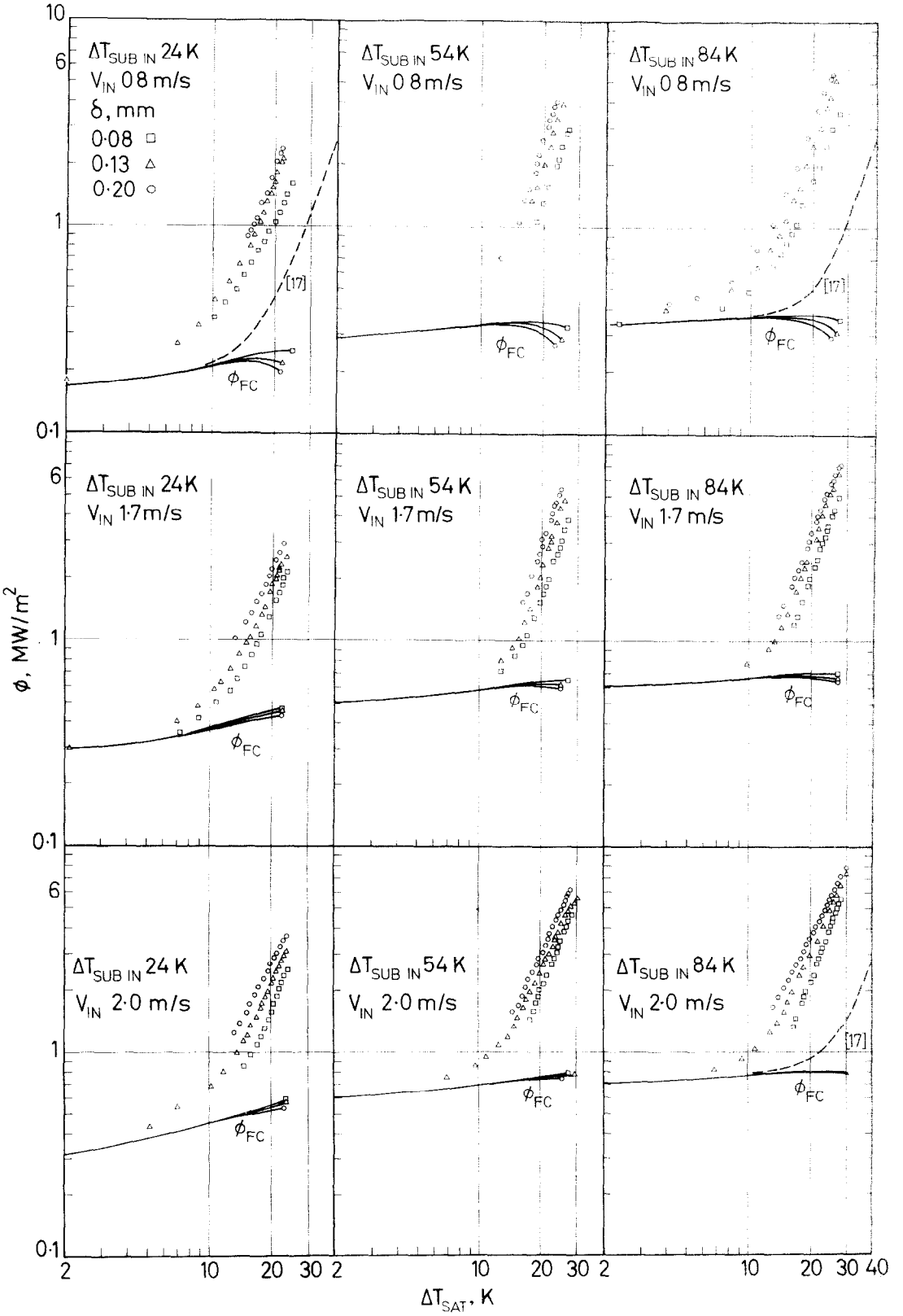

FIG. 2. Subcooled flow boiling curves for water at 116.7 kPa.

simplest possible superposition scheme

$$\phi = \phi_C + \phi_{NB} \tag{3}$$

where ϕ is the measured total flux and the convective flux ϕ_C is calculated from the measured single-phase heat transfer coefficient multipled by the temperature difference [local ΔT_{SAT} + local ΔT_{SUB}].

For given conditions of wall thickness and inlet subcooling the data points for the three flow rates do indeed collapse onto a single nucleate boiling curve within ± 1 K for the most part, Fig. 3. The scatter increases at very low flux when $\phi_{NB} \leqslant \phi_C$. At high heat fluxes only the data for the combination of lowest flow rate and thinnest wall (0.8 m s^{-1}, 0.08 mm) deviate towards wall superheats lying up to 2.5 K above the general curve.

All runs at 84 K subcooling remained in the bubbly flow regime up to burnout, Fig. 4(a), the bubbles retaining their identities except for occasional coalescences leading to small, short-lived vapour patches. All runs at 24 K subcooling underwent transition from bubbly to slug flow before burnout, Figs. 4(b, c), with indications of nucleation continuing on the wall under the large, moving vapour patches. The change of flow regime does not affect the shape of the boiling curves: for the 0.08-mm wall, the data points for ϕ_{NB} in slug flow at 1.7 m s^{-1} and in bubbly flow at 2.0 m s^{-1} coincide over the range 10^6–1.5×10^6 W m^{-2}. Nor does the transition explain the small deviation of the (0.8 m s^{-1} 0.08 mm) data which occurs entirely in bubbly flow at 84 K subcooling and commences below the transition at 24 K subcooling.

This simple superposition scheme appears to account for the influence of flow rate but it leads to separate nucleate boiling curves for each combination of wall thickness and inlet subcooling, summarised in Fig. 5, instead of a single curve dependent only on pressure and, probably, surface conditions. Over the range of conditions in this study the effects of subcooling and wall thickness are similar in magnitude: in combination they change the wall superheat from 14 to 22 K at a nucleate boiling flux of 10^6 W m^{-2}. These significant effects must be considered in any general correlation of subcooled flow boiling data from different sources.

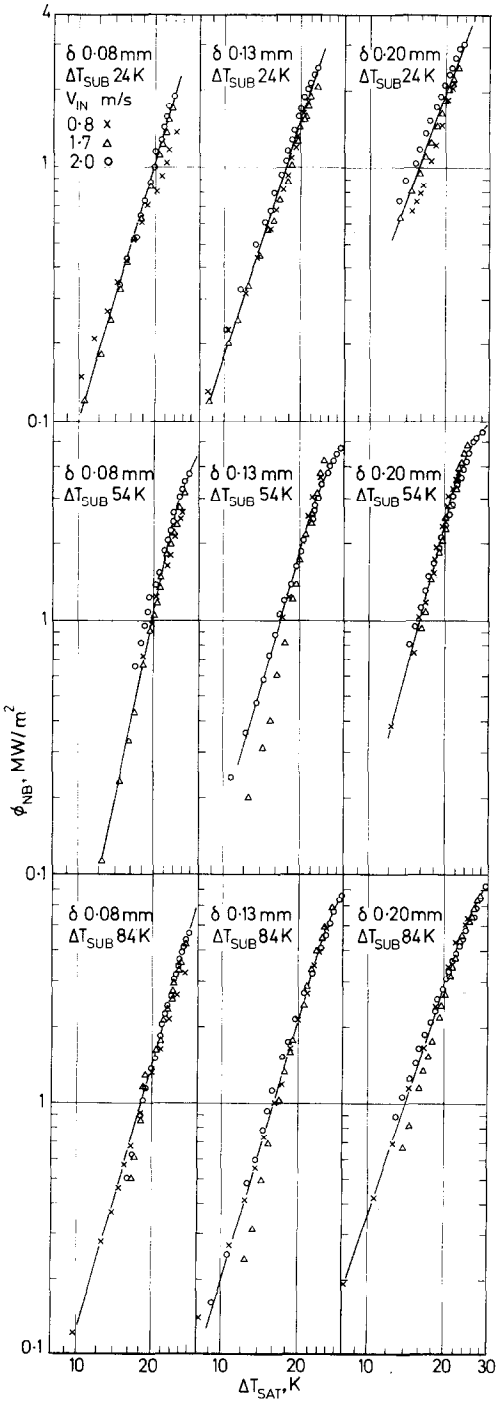

FIG. 3. Nucleate boiling curves.

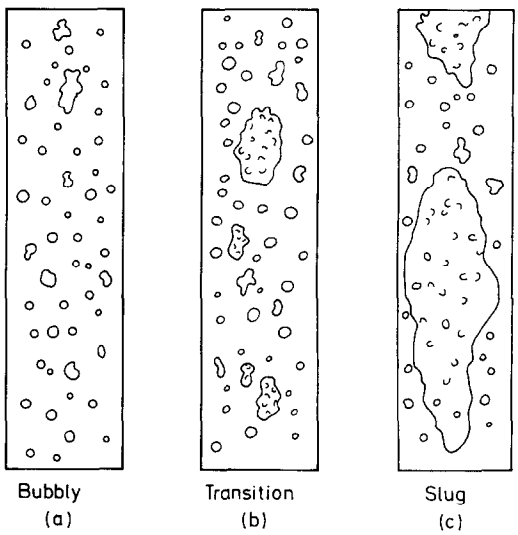

FIG. 4. Flow regimes.

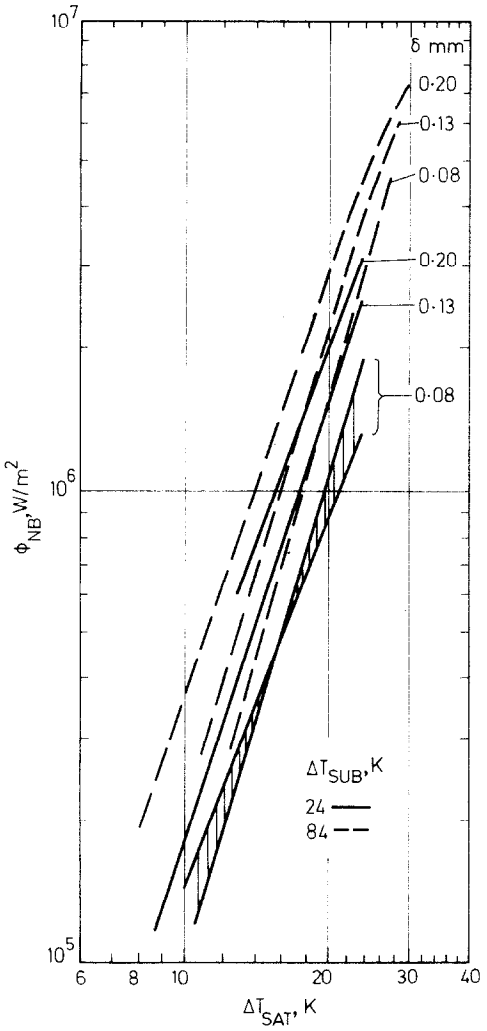

FIG. 5. Nucleate boiling curves: summary.

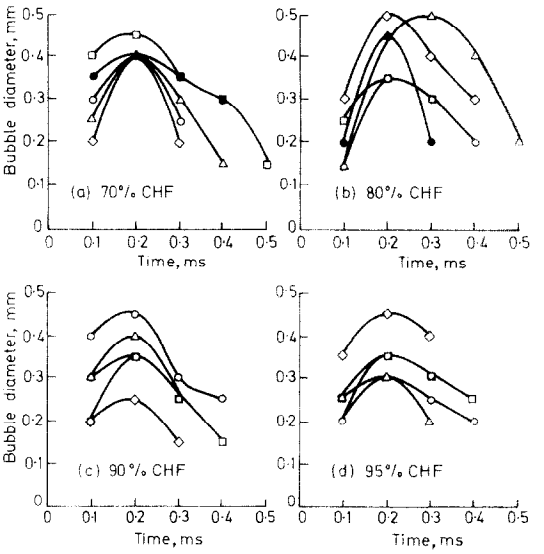

FIG. 6. Bubble growth curves.

4. PHOTOGRAPHIC STUDY

4.1. *General conditions*

High speed cine films were taken at increasing heat fluxes of 70, 80, 90 and 95% of the critical flux (4.92 MW m^{-2}) on the same 0.08-mm-thick test section at 1.7 m s^{-1} and 84 K inlet subcooling. These conditions were chosen for detailed study because the flow regime remained in bubbly flow, giving a clear view of the surface even at the maximum flux. The films were taken at the maximum camera speed of 10^4 frames s^{-1} with the camera directed normal to a 10-mm square of the surface 20 mm from the downstream electrode. Printed enlargements of 40 consecutive frames from each film were analysed. The positions of all active nucleation sites within the 10 mm square were recorded. The bubble frequency, waiting time and growth–collapse curves were measured for bubbles from 30 sites chosen at random on each film.

4.2. *Bubble growth*

Even at the maximum camera speed, individual bubbles appeared in only 3–5 frames. Bubble growth–collapse appeared to be approximately symmetrical in time, Fig. 6. The visible lifetimes were recorded so the true lifetimes were understimated by about 0.1 ms. The poor accuracy of measurement precluded detailed statistical analysis but the frequency of occurrence of short-lived bubbles increased with increasing heat flux, Fig. 7.

The waiting times between successive bubbles lay in the range 0.9–2.9 ms so the camera framing speed introduced less uncertainty than in bubble lifetimes. The measurements were consistent with a normal distribution (according to χ^2 tests at 5% level of significance), Fig. 8. The mean waiting time decreased with increasing heat flux. The total bubble periods (lifetime + waiting time) were not consistent with either a normal or a Poisson distribution [1].

Bubble size was measured as the mean of the axial

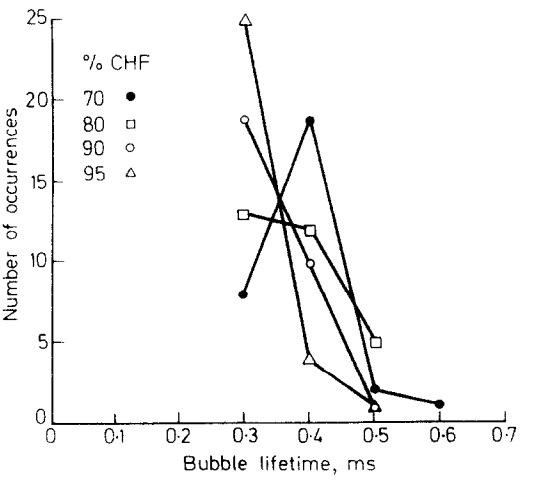

FIG. 7. Bubble lifetime.

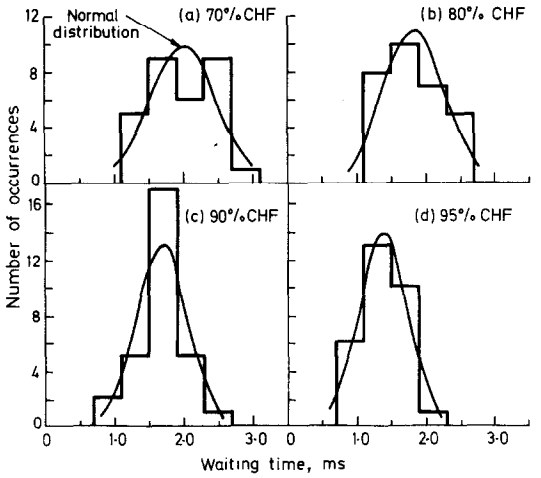

FIG. 8. Waiting times between bubbles.

and transverse dimensions; all bubbles were nearly circular in plan. The maximum diameters were normally distributed (class interval 0.1 mm) with a mean value of 0.4 mm $\pm$ 5% independent of heat flux, Fig. 9. Tolubinsky and Kostanchuk [18] also found the bubble size to be independent of heat flux in subcooled flow boiling.

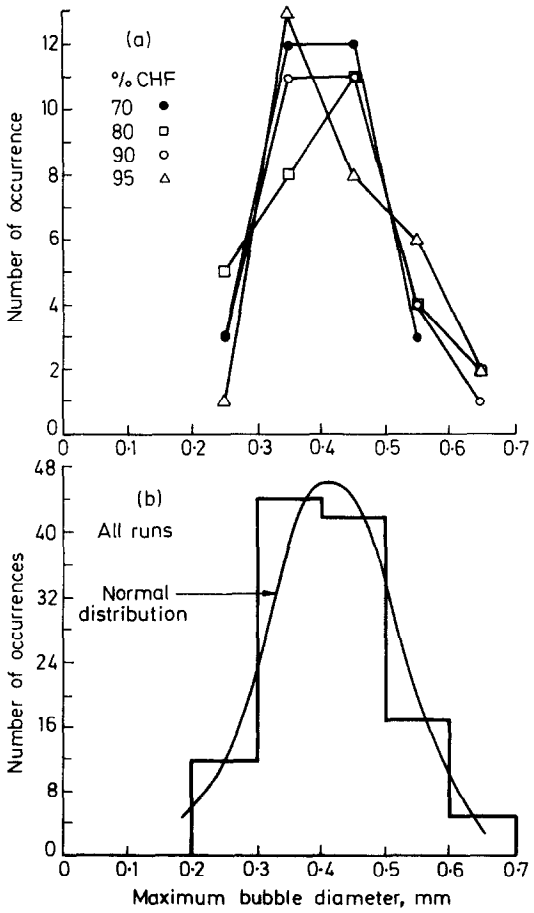

FIG. 9. Bubble sizes.

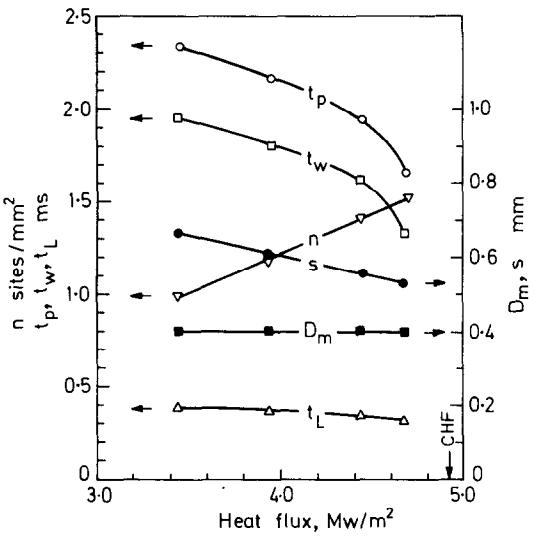

FIG. 10. Mean bubble parameters: variation with heat flux.

The variation of the mean growth parameters with heat flux is summarised in Fig. 10.

4.3. *Distribution of active nucleation sites*

The position of every active site within the 10 x 10 mm square was plotted at the four heat flux levels, Fig. 11. The activation of sites did not proceed in a regular manner with increasing heat flux. Many sites active at a low heat flux became inactive when the heat flux was increased, some becoming active again at a still higher heat flux, Table 1. Of the total of 256 recorded sites, only 152 were active at the highest heat flux. Indications of this behaviour have been noted previously in subcooled flow boiling [10] but studies of pool boiling [19, 20] have suggested that the population of active sites

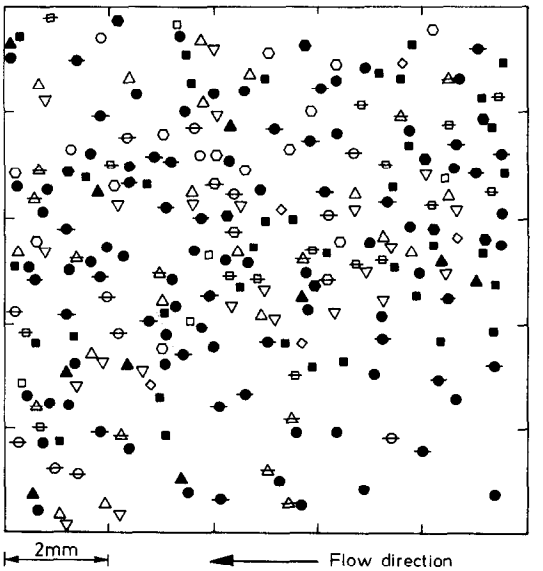

FIG. 11. Spatial distributions of active nucleation sites. (For definition of symbols see Table 1.)

Table 1. Nucleation site activation histories. ΔT_{SUBIN} 84 K, V_{IN} 1.7 m s^{-1}, δ 0.08 mm, CHF 4.92 MW m^{-2}

Heat flux (% CHF)				Active nucleation sites cm^2 (cm^{-2})
70	80	90	95	
√	√	√	√	33 ●
√	√	√	√	15 △
√	√	√	√	16 ⊟
√		√	√	3 ⊖
	√	√	√	12 ⊖
√	√			15 △
√		√		4 □
√			√	3 ○
	√	√		13 ◌
	√		√	5 ◇
		√	√	23 ▽
√				10 ▲
	√			9 ⬢
		√		38 ■
			√	57 ●
99	118	141	152	256

Symbols refer to Figure 11.

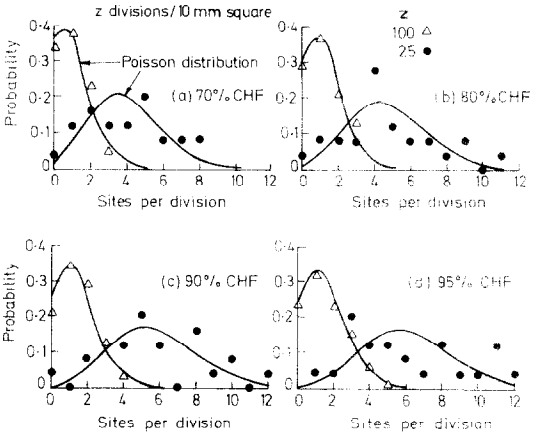

FIG. 12. Distribution of active nucleation sites in subdivisions of surface area.

increases with increasing heat flux by straightforward addition of new sites, without deactivation. It is important to understand the conditions for deactivation, which may invalidate the customary assumption that the population of active sites depends only on the surface roughness and the wall superheat.

Some deactivation might be expected through processes generated by the nucleation site itself, e.g. chance penetration of liquid further than usual after the departure of a bubble, either filling the site entirely with liquid or leaving the liquid–vapour interface in a position requiring a higher superheat for reactivation. A site would be particularly vulnerable if it had been activated at an unusually low superheat by chance coverage by vapour from another site: a very small number of bubbles sliding along the surface were observed in this study but the vast majority of bubbles grew and collapsed at their own nucleation sites.

Alternatively, deactivation may be caused by adjacent active sites creating less favourable conditions for sustained nucleation: a decrease in wall temperature or an increase in the temperature gradient in the liquid. Such interference between sites should alter the spatial distribution of active sites. In the pool boiling studies [19, 20] the distribution was shown to be random by comparing the distribution of populations in subdivisions of the surface with the prediction for a Poisson distribution. According to this test the distributions in the present study are also random, although the agreement with the Poisson distribution depends on the subdivision, Fig. 12. However it has been noted in a previous paper [12] that the distribution of nearest-neighbour distances s provides a more sensitive test of randomness. For a Poisson distribution with a mean density n sites per unit area the probability density for s is given by [21]

$$P(s, s+\mathrm{d}s) = 2\pi n \cdot s \cdot \mathrm{e}^{-n\pi s^2}\,\mathrm{d}s. \qquad (4)$$

The measurements of s in this study deviate quite markedly from equation (4), Fig. 13. Very few sites lie within 0.35 mm of another active site, whereas a random distribution should have a large population of sites in the range $0 \leqslant s \leqslant 0.35$ mm. The cut-off in s occurs at about twice the maximum bubble radius and in [12] we referred to the *inhibition* of nucleation within the area of influence of an active site. Although this terminology describes the end result correctly, it masks the complexity of the processes involved. Examination of the placing of sites newly activated by an increase in heat flux shows that nucleation is *promoted* in the close vicinity of already-active sites but many of the old sites are then deactivated. This exchange of activity between adjacent sites produces the net increase in population with increasing heat flux summarised in Table 1.

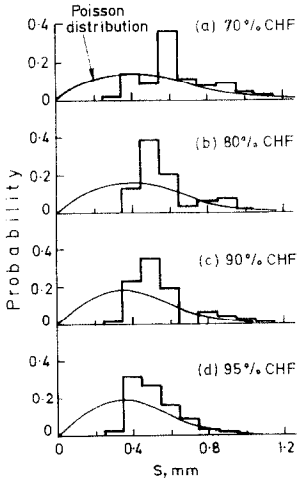

FIG. 13. Distribution of nearest-neighbour distances between active nucleation sites.

The evidence for promotion of new nucleation near old sites during the three flux increases (a) 70–80%, (b) 80–90% and (c) 90–95% CHF comes from comparison of the distributions of nearest distances (i) between all sites active at the lower flux (as in Fig. 13) and (ii) between the new sites at the higher flux and all the sites active at the lower flux. If there is an inhibition mechanism only, the distributions should be similar. For the first increase (a) the distribution for new sites is biassed slightly towards smaller s, Fig. 14(a). For increases (b) and (c) at higher site densities the differences between the distributions are much greater: there is a high probability that new sites lie within 0.15–0.35 mm of a previously-active site, Figs. 14(b, c).

The evidence for suppression comes from the fraction of sites active at the lower flux which survive the increase. The survival probability depends on the distance from a newly-activated site, ranging from zero for $s < 0.25$ mm to about 0.7 for $s > 0.5$ mm. The value 0.7 at large s represents the probability of a site surviving self-deactivation and deactivation by sites coexisting at the lower flux (Fig. 15).

This analysis of nearest-neighbour distances cannot tell the whole story. Some sites must fall under the simultaneous influence of several neighbours: this was characteristic of a considerable number of the sites which were deactivated at a lower heat flux only to become active again at a higher flux. The analysis is based on a small time sample at each level of heat flux: observations over a long period at constant heat flux might also reveal exchanges of activity between adjacent sites. It has been assumed that the nucleation characteristics of the boiling surface did not change over the duration of the experiments at four different heat fluxes. Corrosion–erosion of the stainless-steel surface is not expected under these conditions but Aounallah [22] found that the nucleation characteristics of a new surface were modified by the deposition of a very thin layer of silica from the low concentration dissolved in the water. A substantial

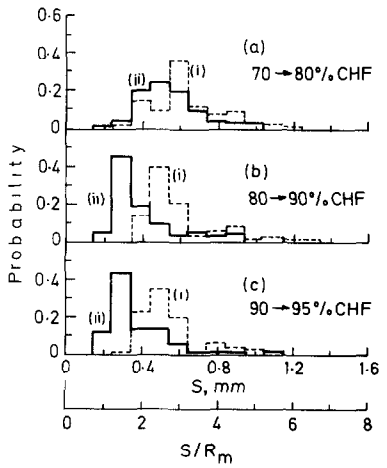

FIG. 14. Distribution of nearest distances between (i) all sites active at lower flux; and (ii) new sites at higher flux and all sites at lower flux.

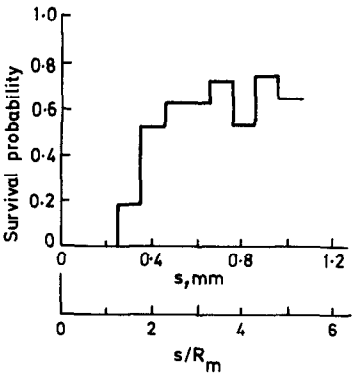

FIG. 15. Probability of site surviving an increase in heat flux, relative to distance s from nearest newly active site. (Combined data for two 10% increases and one 5% increase.)

reduction in contact angle was produced by less than 5 min of boiling. Prolonged boiling over several days produced thin patches of silica within the projected area of bubbles [14]. In the present experiments the heat flux was increased at 15-min intervals, during which time the wall temperatures settled to constant values. Experiments on a similar timescale by Eddington [10, 14] showed that 90% of the nucleation sites deactivated by an increase in heat flux were reactivated when the heat flux was reduced again. Therefore changes in surface conditions should have little effect on the present observations.

It has been shown that an active nucleation site influences other sites over a distance of 2–2.5 times the maximum bubble radius. Conditions in the immediate vicinity of an active site favour the initiation of nucleation at other sites but the simultaneous activity of sites within 1.5–2 bubble radii of each other cannot be sustained. Consequently the net increase in the population of active sites with increasing heat flux involves the deactivation of some of the sites active at low flux and their replacement by a somewhat larger number of new sites. Any calculation utilizing the size distribution of surface cavities without allowance for interference will overpredict the population of active nucleation sites at large wall superheats.

HEAT TRANSFER MODEL

5.1. *Heat transfer zones*

The heated wall is divided into four zones, Fig. 16, with different mechanisms of heat transfer:

Maximum bubble projected area—microlayer evaporation and transient conduction.
Surrounding areas of influence—transient conduction.
Overlapping areas of influence—enhanced transient conduction.
Non-boiling area—single-phase forced convection.

The total heat flux is obtained by summing the contributions of the four zones, calculated by the methods outlined in the following sections.

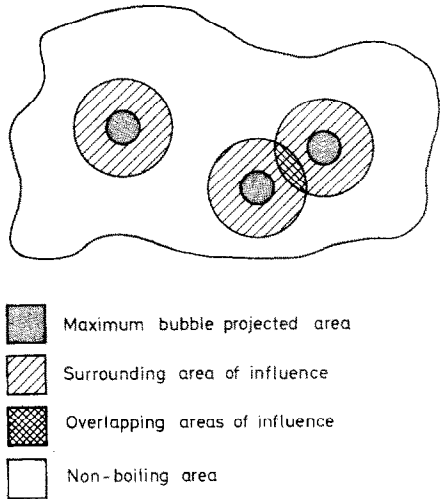

FIG. 16. Heat transfer zones.

5.2. *Maximum bubble projected area*

The fraction F of the surface covered by the maximum bubble projected areas is calculated from the measured density of active nucleation sites n and the mean measured maximum bubble radius R_m, assumed to be the same for all sites,

$$F = \pi R_m^2 n. \tag{5}$$

Overlap of the projected areas is discounted in the light of the observed inhibition of site activity at spacings less than $2R_m$, which also implies negligible bubble coalescence.

All bubbles are assumed to grow and collapse as hemispheres in contact with the wall, with the mean measured values of lifetime t_L and period t_P. For convenience of calculation the growth curves of Fig. 6 are approximated by the expression

$$\frac{R}{R_m} = 4\left(\frac{t}{t_L}\right)\left(1-\frac{t}{t_L}\right) \tag{6}$$

corresponding to symmetrical growth–collapse with respect to time. The assumption of hemispherical growth is supported by the generalised shape history developed by Cooper *et al.* [23] for bubble growth on a wall in uniformly superheated liquid, which predicts hemispherical growth for $t^+ < 10^{-2}$, where

$$t^+ = \frac{t_0\sigma^2}{b^6\rho_l^2}, \quad b = Ja\,\alpha_l^{1/2}. \tag{7}$$

In this photographic study the growth times to maximum radius corresponded to $t^+ < 10^{-3}$. Again following [23], over this time range the initial thickness of the liquid microlayer formed under the bubble is given approximately by

$$\delta_{MO} = 0.8(\nu_l t_0)^{1/2}. \tag{8}$$

The microlayer is initially at the wall temperature but the liquid–vapour interface falls immediately to the saturation temperature. Evaporation proceeds due to the wall superheat ΔT_{SAT} (assumed constant and uniform), either until the microlayer evaporates to dryness or until bubble collapse restores contact between the wall and the bulk liquid. Any period during which the wall is in direct contact with vapour is assumed to be adiabatic. The assumption that the hemispherical shape is maintained during collapse probably leads to an overestimate of the delay before the return of bulk liquid: Cooper and Chandratilleke [24] have shown that bubbles growing into subcooled liquid round off during collapse.

Heat transfer across the microlayer is approximated by a two-stage calculation. Initially the microlayer evaporates as if it were semi-infinite and no effect reaches the wall until after a delay time t_D given by

$$t_D = 0.6\,\delta_{MO}^2/\alpha_l, \tag{9}$$

$$\frac{t_D}{t_0} = 0.384\,Pr. \tag{10}$$

Subsequently heat transfer is calculated for a linear temperature gradient across the microlayer

$$\phi = k_l\Delta T_{SAT}/\delta_M. \tag{11}$$

The value 0.6 for the constant in equation (9) was chosen by equating the approximate calculation with the analytical solution for transient conduction across a slab of constant thickness [1]. The microlayer thickness decreases due to evaporation. During the first stage the decrease ε is negligible for the conditions of these experiments:

$$\frac{\varepsilon}{\delta_{MO}} = 2\left(\frac{0.6}{\pi}\right)^{1/2} C_l\Delta T_{SAT}/\lambda \tag{12}$$

$$\cong 0.05. \tag{13}$$

During the second stage

$$\frac{d\delta_M}{dt} = -\frac{k_l\Delta T_{SAT}}{\rho_l\lambda\delta_M} \tag{14}$$

and evaporation to dryness occurs after a time t_E given by

$$t_E = \frac{\delta_{MO}^2\rho_l\lambda}{2k_l\Delta T_{SAT}}, \tag{15}$$

$$\frac{t_E}{t_0} = 0.32\frac{\lambda\,Pr}{c_l\Delta T_{SAT}}. \tag{16}$$

An annular element of wall area R to $R+dR$ is subjected to a cycle of heat transfer, Fig. 17, which depends on the value of t_0 given by equation (6):

(A) If $t_D + t_E < t_L - 2t_0$:

(i) conduction across the microlayer for time t_E;
(ii) no heat transfer for $t_L - 2t_0 - t_D - t_E$;
(iii) quenching by semi-infinite bulk liquid, initially at T_B, for $t_Q = t_P - t_L + 2t_0 + t_D$.

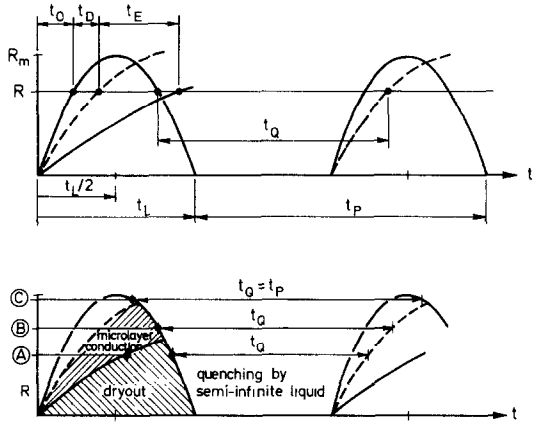

FIG. 17. Heat transfer sequences on bubble projected areas.

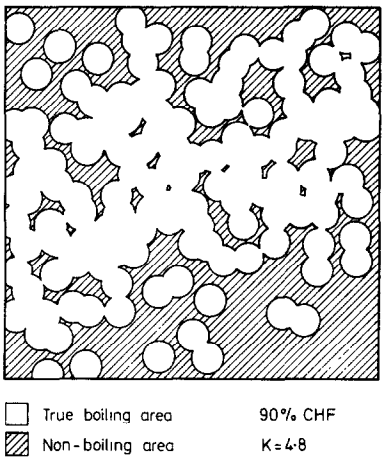

FIG. 18. Determination of true boiling area.

(B) If $t_D + t_E > t_L - 2t_0$:

(i) conduction across the microlayer for $t_L - 2t_0 - t_D$;
(ii) quenching by bulk liquid for $t_Q = t_P - t_L + 2t_0 + t_D$.

(C) If $t_D > t_L - 2t_0$:

(i) quenching by bulk liquid for $t_Q = t_P$.

Heat transfer across the microlayer is calculated from equations (11) and (14). The mean heat flux during quenching is

$$\bar{\phi}_Q = \frac{2k_l(\Delta T_{SAT} + \Delta T_{SUB})}{(\pi\alpha_l t_Q)^{1/2}}. \quad (17)$$

The heat transfer is calculated over a bubble period and then integrated over the circular area $0 < R < R_m$. Details of the calculation are given in [1].

5.3. *Areas of influence*

In the simplest quenching heat transfer model an area K times the maximum bubble projected area is subjected uniformly to the heat flux given by equation (17) with t_Q equal to the bubble period t_P. Conventionally K is expected to have a value of about 4. The nominal boiling fraction of the wall area is KF; single-phase heat transfer occurs over the fraction $1 - KF$. The areas of influence as defined in this paper would occupy a fraction $(K-1)F$.

However, this takes no account of the significant degree of overlap of areas of influence at high site densities if K is indeed about 4. The true boiling area is only a fraction X of the nominal area and the fraction of the surface associated with single-phase convection is increased to $1 - XKF$. The reduction in boiling area is offset by the enhanced heat flux on the overlapping areas, caused by the increased frequency of quenching by two or more sites [1, 12]. In [12] we attempted to calculate the overlap for different degrees of interference between sites. Here the true boiling area is measured directly by drawing circles corresponding to different values of K round the known positions of active nucleation sites, e.g. Fig. 18, since the appropriate value of K is not known *a priori*. Fortunately X depends primarily on KF with little dependence on K alone, Fig. 19, so this graph can be used for intermediate values of K.

The overlapping areas of influence occupy a fraction $(1-X)KF$ of the wall area. For simplicity only binary overlap is assumed: the simultaneous interaction of three or more sites is neglected. For quenching by two sites having the same frequency but independent timing for the start of bubble growth the mean heat flux is increased to 4/3 times the flux given by equation (17) with $t_Q = t_P$ [1, 12].

The areas of influence without overlap (and excluding the area under the bubbles) occupy a fraction $(2X-1)KF - F$ of the wall area. The mean heat flux is given by equation (17).

5.4. *Non-boiling area*

The single-phase convective flux on the fraction $1 - XKF$ of the wall area is calculated from the James *et al.* correlation [15].

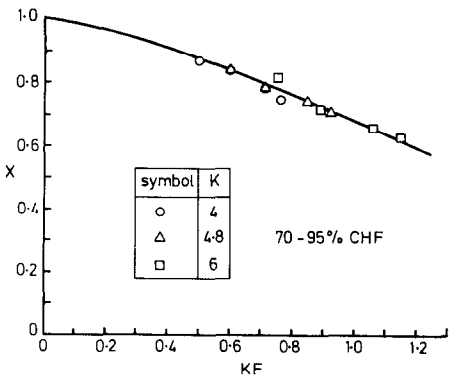

FIG. 19. Dependence of ratio X of true to nominal boiling area on nominal boiling area KF.

6. HEAT TRANSFER CALCULATIONS

6.1. *Calculations by the Section 5 model*

The components of the wall heat flux were calculated for the conditions of the four cine films, using the measured wall temperatures, bubble growth parameters and nucleation site densities described in Section 4. The bulk liquid temperature was taken to be the value at inlet. The only unspecified quantity in the theoretical expressions was the factor K determining the ratio of the area of influence to the maximum bubble projected area. K was adjusted to make the total calculated heat flux equal to the measured flux: the required value varied from 7.5 at the lower fluxes to 5.8 at the highest flux, Table 2.

The contribution to the total heat flux from microlayer evaporation was only 2–3%. Single-phase convection accounted for 10% decreasing to 5% as the boiling area increased at higher fluxes. By far the most important mechanism of heat transfer was the transient conduction on the combined bubble projected area and surrounding area of influence.

6.2. *The transient conduction heat flux*

The use of transient conduction to a semi-infinite medium to model the periods when the wall is in direct contact with the bulk liquid leads to values of K which are much larger than the conventional value 4 used in pool boiling calculations. The corresponding nominal boiling areas ($K \times$ bubble projected area $\times$ number of sites) actually exceed the surface area at the higher heat fluxes, Table 2. However, the non-uniform distribution of nucleation sites causes a large degree of overlap of the areas of influence so that the true boiling area only covers about three-quarters of the surface. Without the allowance for the increased frequency of transient conduction on overlapping areas the deduced values of K would be even higher.

The examination of interference between nucleation sites in Section 4.3 suggests that the influence of an active site declines gradually over a distance of about 2.5 R_m ($K \cong 6.25$). We do not yet understand the link between interference and the heat transfer processes round a site but this limited evidence suggests that it may be physically unrealistic to assume that the quenching heat flux is uniformly distributed over areas as large as $K \geqslant 6$. If so, the intensity of the heat flux closer to the nucleation sites must be increased in compensation. There is no reason to expect the transient conduction model, equation (17), to *accurately* represent the quenching process: if bubble-induced convection is sufficiently strong to produce the instantaneous replacement of liquid which the model requires, it is likely to increase the subsequent rate of heat transfer. Improvement of the theoretical model must await detailed investigations of the wall temperature variations near groups of active nucleation sites, discussed in [9].

This part of the investigation has been limited in the range of conditions studied and in the accuracy of measurement of some of the bubble parameters. Average values have been substituted into the theoretical expressions without investigation of possible correlations, e.g. between bubble size and frequency, which might affect the average values of products. Within these limitations, the transient-conduction model has been shown to give the right magnitude for the dominant mechanism of heat transfer. The model cannot be used for accurate calculations without additional information about the effective size of the area of influence, since the value of K is not constant.

6.3. *Microlayer evaporation*

Under the conditions of this study microlayer evaporation makes a negligible direct contribution to the wall heat flux. However it plays a vital role in the bubble motion which drives the quenching heat flux. At each of the four heat fluxes the rate of vapour generation by microlayer evaporation is six times the generation rate given by the product of bubble frequency and maximum volume: bubble growth and collapse must depend on a delicate imbalance between simultaneous evaporation from the microlayer and condensation on the bubble cap.

6.4. *Single-phase convection*

In the nucleate boiling dominated conditions of this study accuracy in calculating the convective contribution is not important. In that they are based on fully-developed turbulent flow in a smooth-walled channel, neither the calculations for the correlation scheme in Section 3.2 nor those for the mechanistic model in Section 5.4 can be physically realistic for small areas of wall surrounded by highly active nucleation sites. A

Table 2. Calculated heat flux components (MW m^{-2})

CHF (%)	K	KF	KFX	Microlayer evaporation	Quenching under bubble	Quenching, area of inf.	Convection	ϕ Total	ϕ Experimental
70	7.5	0.94	0.67	0.06	0.49	2.64	0.28	3.47	3.44
80	7.3	1.08	0.73	0.08	0.62	3.03	0.23	3.96	3.94
90	6.7	1.19	0.74	0.10	0.80	3.29	0.23	4.42	4.43
95	5.8	1.10	0.73	0.13	0.93	3.38	0.24	4.68	4.67

better model is required for the interaction of convective and nucleate boiling heat fluxes of similar magnitude.

7. CONCLUSIONS

The following conclusions are based on the conditions of this particular study and do not necessarily apply to all conditions of subcooled flow boiling.

1. The rate of nucleate boiling heat transfer at a given wall superheat increases with increasing wall thickness and with increasing subcooling.
2. The influence of flow rate is represented satisfactorily by a simple superposition model $\phi = \phi_{NB} + \phi_C$, provided $\phi_{NB} > \phi_C$. The heat transfer rate is not sensitive to a change of flow regime from bubbly to slug flow.
3. Further investigation is required of the effect of surface conditions on subcooled flow boiling.
4. The probability of activation of new bubble nucleation sites is increased within 1.25–1.75 bubble radii of already-active sites.
5. The activation of new sites tends to deactivate the old sites, the influence declining over a distance of 2.5 bubble radii.
6. As consequences of conclusions 4 and 5, many sites active at lower wall superheats become inactive at higher superheats and the spatial distribution of sites is not random. An understanding of the interactions between sites is necessary for the prediction of the active site distribution as a function of wall superheat and the size distribution of potential sites.
7. Heat transfer occurs primarily by bubble-induced quenching of the wall by cold liquid. Microlayer evaporation makes a negligible direct contribution to the heat flux but it may exert an important indirect influence through its effect on bubble dynamics.
8. The quenching flux may be modelled by repeated transient conduction to semi-infinite liquid over an area of influence 5.8–7.5 times the bubble projected area, with allowance for the large reduction in boiling area due to overlap of areas of influence and the increased frequency of quenching on the overlapping areas. However, conclusion 5 suggests that it may be unrealistic to assume uniform quenching right up to the edge of an area of influence as large as seven times the bubble area.
9. The predictive capability of the theoretical model is impaired by the apparent variation in the size of the area of influence. Further investigation is required of the processes of heat transfer near groups of active nucleation sites.

Acknowledgements—This work was supported by the Science and Engineering Research Council and by UKAEA Harwell. V. H. Del Valle received support from the Consejo Nacional de Ciencia y Tecnologia, Mexico.

REFERENCES

1. V. H. Del Valle M., Flow boiling near the critical heat flux. D. Phil. thesis, Oxford University (1980).
2. G. Guglielmini and E. Nannei, On the effect of heating wall thickness on pool boiling burnout, *Int. J. Heat Mass Transfer* **19**, 1073–1075 (1976).
3. M. P. Fiori and A. E. Bergles, Model of critical heat flux in subcooled flow boiling, Report No. DSR 70281-56, Department of Mechanical Engineering, Massachusetts Institute of Technology (1968).
4. F. E. Tippets, Critical heat flux and flow pattern characteristics of high pressure boiling water in forced convection, *J. Heat Transfer* **86**, 12–22 (1964).
5. G. F. Hewitt, H. A. Kearsey, P. M. C. Lacey and D. J. Pulling, Burnout and film flow in the evaporation of water in tubes, *Proc. Instn mech. Engrs* **180** (3c), 206–215 (1965).
6. U. Magrini and E. Nannei, On the influence of the thickness and thermal properties of heating walls on the heat-transfer coefficients in nucleate pool boiling, *J. Heat Transfer* **97**, 173–178 (1975).
7. V. A. Grigoriev, Yu. M. Pavlov, Ye. V. Ametistov, A. V. Klimenko and V. V. Klimenko, Concerning the influence of thermal properties of heating surface material on heat transfer intensity of nucleate pool boiling of liquids including cryogenic ones, *Cryogenics* **17**, 94–96 (1977).
8. T. L. Chuck and J. E. Myers, The effect of heater plate thickness on boiling heat-transfer coefficients, *Int. J. Heat Mass Transfer* **21**, 187–191 (1978).
9. D. B. R. Kenning, Wall temperatures in nucleate boiling, Report No. OUEL 1530/84, Department of Engineering Science, Oxford University (1984).
10. R. I. Eddington and D. B. R. Kenning, The prediction of flow boiling bubble populations from gas bubble nucleation experiments, *6th Int. Heat Transfer Conference*, Toronto, Vol I, pp. 275–280 (1978).
11. R. L. Judd and K. S. Hwang, A comprehensive model for nucleate pool boiling heat transfer including microlayer evaporation, *J. Heat Tranfer* **98**, 623–629 (1976).
12. D. B. R. Kenning and V. H. Del Valle M., Fully developed nucleate boiling: overlap of areas of influence and interference between bubble sites, *Int. J. Heat Mass Transfer* **24**, 1025–1032 (1981).
13. R. I. Eddington, D. B. R. Kenning and A. I. Korneichev, Comparison of gas and vapour bubble nucleation on a brass surface in water, *Int. J. Heat Mass Transfer* **21**, 855–862 (1978).
14. R. I. Eddington, Comparisons between gas and vapour bubble nucleation at a heater surface. D. Phil. thesis, Oxford University (1978).
15. D. D. James, B. W. Martin and D. G. Martin, Forced convection heat transfer in asymmetrically heated ducts of rectangular cross-section, *3rd Int. Heat Transfer Conference*, Chicago, Vol. I, p. 85 (1966).
16. D. B. R. Kenning and Y-S. Kao, Forced convection heat transfer to water containing gas bubbles: enhancement not dependent on thermocapillarity, *Int. J. Heat Mass Transfer* **15**, 1709–1717 (1972).
17. R. W. Bjorge, G. R. Hall and W. M. Rohsenow, Correlation of forced convection boiling heat transfer data, *Int. J. Heat Mass Transfer* **25**, 753–757 (1982).
18. V. I. Tolubinsky and D. M. Kostanchuk, Vapour bubble growth rate and heat transfer intensity in subcooled water boiling, *4th Int. Heat Transfer Conference*, Paris, Vol. V, Paper B2.8 (1970).
19. R. F. Gaertner and J. W. Westwater, Population of active sites in nucleate boiling heat transfer, *Chem. Engng Prog. Symp. Series* Vol. 56, No. 39, pp. 39–48 (1960).
20. M. Sultan and R. L. Judd, Spatial distribution of active sites and bubble flux density, *J. Heat Transfer* **100**, 56–62 (1978).
21. R. F. Gaertner, Distribution of active sites in the nucleate

boiling of liquids, *Chem. Engng Prog. Symp. Series* Vol. 59, No. 41, pp. 52–61 (1963).
22. Y. Aounallah, Heat transfer in annular two-phase flow. D. Phil. thesis, Oxford University (1982).
23. M. G. Cooper, A. M. Judd and R. A. Pike, Shape and departure of single bubbles growing at a wall, *6th Int. Heat Transfer Conference*, Toronto, Vol. I, pp. 115–120 (1978).
24. M. G. Cooper and T. T. Chandratilleke, Growth of diffusion-controlled vapour bubbles at a wall in a known temperature gradient, *Int. J. Heat Mass Transfer* **24**, 1475–1492 (1981).

EBULLITION A HAUT FLUX THERMIQUE D'UN ECOULEMENT SOUS-REFROIDI

Résumé—Dans une recherche expérimentale de l'ébullition nucléée d'un écoulement sous-refroidi d'eau à la pression atmosphérique sur l'acier inoxydable, il est trouvé que le coefficient de transfert thermique croît avec l'augmentation du sous-refroidissement et aussi avec l'accroissement de l'épaisseur de la paroi dans le domaine 0,08–0,20 mm. La taille de bulle, la fréquence et la distribution des sites de nucléation sont mesurées à une vitesse d'entrée 1,7 m s^{-1}, à 84 K de sous-refroidissement, pour une épaisseur de paroi de 0,08 mm et des flux thermiques à 70–95% du flux critique. Les observations s'accordent avec un modèle de transfert thermique principalement dû à une trempe de la surface à la fréquence des bulles et augmenté par une convection monophasique et par une petite contribution de l'évaporation de micro-couche. Bien que la population totale de sites de nucléation augmente avec la surchauffe de la paroi, le démarrage de nouveaux sites désactive beaucoup de sites actifs à de plus faibles surchauffes.

UNTERKÜHLTES STRÖMUNGSSIEDEN BEI HOHEN WÄRMESTROMDICHTEN

Zusammenfassung—Bei experimentellen Untersuchungen des unterkühlten Strömungssiedens von Wasser bei Atmosphärendruck an rostfreiem Stahl wurde festgestellt, daß der Wärmeübergangskoeffizient mit größer werdender Unterkühlung zunimmt und ebenso mit steigender Wandstärke im Bereich von 0,08 bis 0,20 mm. Gemessen wurden Blasengröße, Frequenz und Verteilung der Siedekeime bei einer Eintrittsgeschwindigkeit von 1,7 m s^{-1}, einer Unterkühlung von 84 K, einer Wandstärke von 0,08 mm und bei Wärmestromdichten, die 70 bis 95% der kritischen Wärmestromdichte betragen. Die Beobachtungen stimmten mit einem Wärmeübertragungsmodell überein, welches in erster Linie die Oberflächenwiederbenetzung mit der Blasenfrequenz beschreibt, überlagert durch einphasige Konvektion und einen kleinen Anteil 'microlayer'—Verdampfung. Obwohl die Gesamtzahl der Siedekeime mit größer werdender Wandüberhitzung zunimmt, deaktiviert der Start neuer Keimstellen viele bei geringerer Überhitzung aktive Keimstellen.

КИПЕНИЕ НЕДОГРЕТОГО ПОТОКА ПРИ ИНТЕНСИВНОЙ ПОДАЧЕ ТЕПЛА

Аннотация—В результате экспериментального исследования процесса пузырькового кипения недогретого потока воды при атмосферном давлении на нержавеющей стали найдено, что коэффициент теплопереноса увеличивается с ростом недогрева, а также с увеличением толщины стенки в диапазоне 0,08–0,20 мм. Размер пузырька, частота зародышеобразования и распределение мест образования пузырьков измерялись при скорости на входе 1,7 м $с^{-1}$, недогреве 84 К, толщине стенки 0,08 мм и при тепловых потоках, составляющих 70–95% от критического потока. Эксперименты согласуются с моделью теплопереноса, в первую очередь, за счет резкого охлаждения поверхности с частотой зарождения пузырьков, дополняемой однофазной конвекцией и небольшим вкладом испарения микрослоя. Несмотря на то, что полное число зон зарождения пузырьков растет с увеличением перегрева стенки, возникновение новых зон дезактивирует множество ранее активных при небольшом перегреве.